

# Supplementary information for “Understanding single-phase water-management signatures in fuel-cell impedance spectra: A numerical study”<sup>\*</sup>

A. Kosakian<sup>a,b</sup>, L. Padilla Urbina<sup>a,c</sup>, A. Heaman<sup>a</sup>, M. Secanell<sup>a,\*</sup>

<sup>a</sup>*Energy Systems Design Laboratory, Department of Mechanical Engineering, University of Alberta, Canada*

<sup>b</sup>*Department of Mathematical and Statistical Sciences, University of Alberta, Canada*

<sup>c</sup>*Department of Chemical Engineering, University of Alberta, Canada*

## 1. Water uptake by the electrolyte in the catalyst layers

In this work, a novel water-uptake relation was obtained for the fuel-cell catalyst layers by fitting the experimentally measured sorption isotherms for catalyst layers<sup>1,2</sup> and pseudo catalyst layers (PCLs)<sup>3</sup>. The original data and the resulting fits are shown in Figure 1 along with the water-uptake curves for ultrathin Nafion<sup>®</sup> films<sup>4-9</sup>. The latter are shown for comparison only to highlight the discrepancy between the catalyst-layer and thin-film uptake. Their consideration resulted in a significantly worse fit quality and the PEMFC model failing to accurately predict the hydration and resistance dynamics of the cell.

Lines in Figure 1 are the best fits resulting in the following equation with  $R^2$  of at least 0.990 (0.993 on average):

$$\lambda_{\text{eq}} = [6.932a_w - 14.53a_w^2 + 11.82a_w^3] \exp\left(-2509\left(\frac{1}{T} - \frac{1}{303.15}\right)\right). \quad (1)$$

The fitting was performed with the Sequential Least Squares Programming (SLSQP) algorithm available in SciPy<sup>10</sup>. This was done by minimizing the overall residual computed as the  $L_2$  norm of the sum of the squared residuals normalized by the number of the points in each data set so that the data with the larger number of points would not contribute more to the fitting:

$$\text{Residual} = \left\| \left\| \frac{\sum_{i=1}^{N_j} (\lambda_{\text{eq},i}^j - \lambda_{\text{eq},i}^{\text{exp},j})^2}{N_j} \right\| \right\|_2,$$

where the  $L_2$  norm is taken with respect to the data-set index  $j$ .

## 2. Absorbed-water diffusivity in the electrolyte phase of the catalyst layers

Direct substitution of the isotherm (1) into the Darken factor results in a large relation with many terms that is inconvenient to use and analyze. For that reason, a different approach was taken, in which equation 1 was used to generate the equilibrium water content for 1000 values of water activity between  $10^{-12}$  and 1, and natural logarithms of both data arrays were taken. The smallest value of the water activity was chosen so as to limit the natural

---

<sup>\*</sup>This is the authors' preprint of the supporting information for the article published in *Electrochimica Acta* on April 24, 2020 (<https://doi.org/10.1016/j.electacta.2020.136204>).

<sup>\*</sup>Corresponding author

*Email address:* [secanell@ualberta.ca](mailto:secanell@ualberta.ca) (M. Secanell)

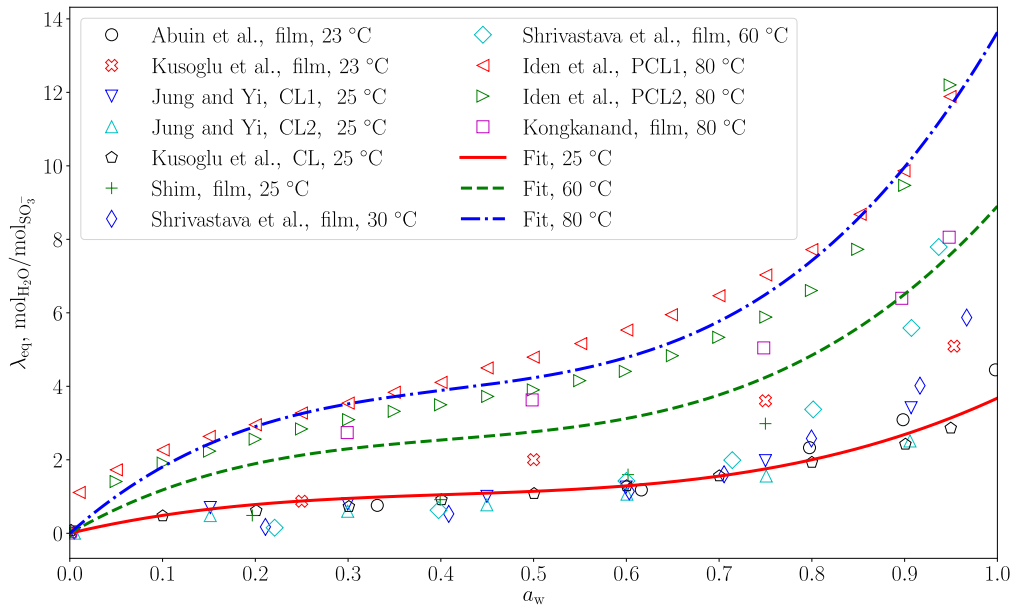


Figure 1: Comparison of the experimentally measured sorption isotherms for catalyst layers, pseudo catalyst layers, ultrathin Nafion<sup>®</sup> membranes, and their fits at the indicated temperature values. Markers represent the data from Abuin et al.<sup>4</sup> (17-nm film on Au), Kusoglu et al.<sup>5</sup> (11-nm film on Au), Jung and Yi<sup>2</sup> (CL1: 0.2 mg<sub>Pt</sub>/cm<sup>2</sup><sub>CL</sub>; CL2: 0.1 mg<sub>Pt</sub>/cm<sup>2</sup><sub>CL</sub>; both on Teflon<sup>®</sup>), Kusoglu et al.<sup>1</sup> (CL with 0.11 mg<sub>Pt</sub>/cm<sup>2</sup><sub>CL</sub> and I/C ratio of 0.8 on PTFE), Shim and coworkers<sup>6,7</sup> (25-nm film on Au), Shrivastava et al.<sup>8</sup> (15-nm film on Pt), Iden et al.<sup>3</sup> (averaged data for GKB and KB PCLs, I/C ratio 0.7-1.3 in all), and Kongkanand<sup>9</sup> (33-nm film on Au). Measurements at the ambient temperature<sup>4,5</sup> were assumed to had been performed at 23 °C. Lines represent the sorption isotherms computed with equation (1).

logarithm  $\ln a_w$ . Then, the derivatives  $\partial \ln a_w / \partial \ln \lambda_{\text{eq}}$  were approximated with the first-order backward differences and plotted against the temperature-corrected water-content values

$$\lambda_{\text{eq,corr}} = \lambda_{\text{eq}} \exp \left( 2509 \left( \frac{1}{T} - \frac{1}{303.15} \right) \right) = 6.932a_w - 14.53a_w^2 + 11.82a_w^3 \quad (2)$$

to remove the temperature dependence from the water-content axis. The exponent in the equation above comes from the isotherm (1). The derivatives  $\partial \ln a_w / \partial \ln \lambda_{\text{eq}}$  were plotted against  $\lambda_{\text{eq,corr}}$ , and the best fits were found using the SLSQP algorithm as

$$\frac{\partial \ln a_w}{\partial \ln \lambda_{\text{eq}}} = \begin{cases} \exp(0.7647\lambda_{\text{eq,corr}}^{2.305}), & \lambda_{\text{eq,corr}} < 1.209; \\ 3.266 + 2.930 [\exp(-6.735(\lambda_{\text{eq,corr}} - 1.209)\lambda_{\text{eq,corr}}^{-0.8994}) - 1], & \lambda_{\text{eq,corr}} \geq 1.209. \end{cases} \quad (3)$$

The  $R^2$  of the fit is 0.999. The fitted Darken factor (3) depends on temperature through  $\lambda_{\text{eq,corr}}$  computed using equation (2). Figure 2 shows the fits of the temperature-corrected and uncorrected data. The distinct peak in the Darken factor is due to the slower water uptake at the intermediate water activities seen in Figure 1. With the known Darken factor, diffusivity of water absorbed into the electrolyte can be computed as discussed in the main text.

### 3. Water uptake by the membrane

Figure 3 illustrates the experimentally measured water uptake curves for various Nafion<sup>®</sup> membranes at different temperature values<sup>1,3,11-14</sup>. While there is some variation in the water uptake with temperature, the exact

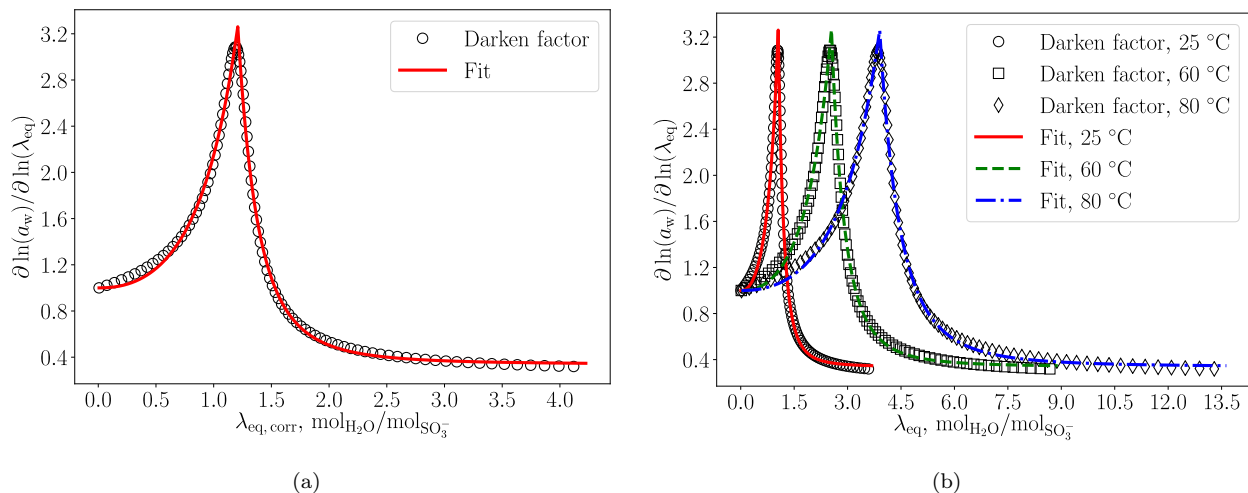


Figure 2: The Darken factor  $\partial \ln a_w / \partial \ln \lambda_{eq}$  computed from the sorption isotherm (1) for catalyst layers (markers) and the corresponding fits with equation (3) (lines). The temperature-corrected data are shown in graph (a). The dependence of the Darken factor on temperature is illustrated in graph (b).

dependence of the equilibrium water content on temperature cannot be established. This goes against the common understanding that the elevated temperature leads to the lower water uptake in the PFSA-based ionomers<sup>15</sup>. At the same time, higher temperature reduces the stiffness of the polymer backbone, allowing for more uptake and swelling<sup>15</sup>. Comparing Figure 1 to Figure 3, one should note that the temperature dependency is more evident in the water uptake curves for catalyst layers and thin ionomer films. This suggests that the chemico-mechanical balance between sorption kinetics and swelling may be different in Nafion<sup>®</sup> confined to ultrathin films and coatings.

The experimental data in Figure 3 were fitted with the SLSQP algorithm in order to obtain an equation for a sorption isotherm suitable for a wide range of Nafion<sup>®</sup> membranes. The fitting procedure resulted in the following equation for the water uptake in Nafion<sup>®</sup> membranes with  $R^2$  of at least 0.992 (average 0.996):

$$\lambda_{eq} = [18.37a_w - 37.46a_w^2 + 31.70a_w^3] \exp\left(-66.28\left(\frac{1}{T} - \frac{1}{303.15}\right)\right). \quad (4)$$

The temperature dependence of equation (4) is weak, as seen in Figure 3, due to the absence of a clear temperature trend in the experimental data. The resulting sorption isotherms at 25–80 °C are almost identical to the water-uptake curve measured by Zawodzinski et al.<sup>11</sup> at 30 °C with the maximum deviation of about 7% at the unit water activity.

#### 4. Absorbed-water diffusivity in the membrane

Since electrolyte hydration is typically described in the fuel-cell models with  $\lambda_{eq}$ -dependent source terms in the catalyst layers (see, for instance,<sup>17–25</sup> and this work), sorption isotherms for membranes are only of interest in terms of their appearance in the Darken factor for computing the back-diffusivity of absorbed water. However, substitution of equation (4) into the Darken factor results in a diffusion coefficient that is similar to that from Motupally et al.<sup>26</sup>, who used Zawodzinski et al.’s<sup>11</sup> isotherm, up to a constant scaling factor. Thus, the diffusivity from Motupally et al. was used in this work and then scaled up for the simulated ohmic resistance of the membrane and electronically conductive components to match the experimental data.

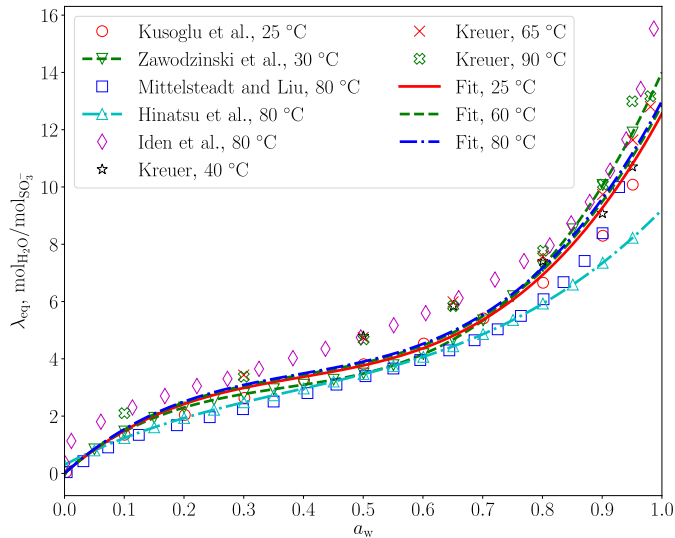


Figure 3: Comparison of the experimentally measured sorption isotherms for Nafion<sup>®</sup> membranes and their fits at the indicated temperature values. Markers represent the data from Kusoglu et al.<sup>1</sup> (Nafion<sup>®</sup> 212 at 25 °C), Zawodzinski et al.<sup>11</sup> (Nafion<sup>®</sup> 117 at 30 °C, fit by Springer et al.<sup>16</sup>), Mittelsteadt and Liu<sup>12</sup> (Nafion<sup>®</sup> 112 at 80 °C), Hinatsu et al.<sup>13</sup> (Nafion<sup>®</sup> 117 and 125 at 80 °C, their own fit), Iden et al.<sup>3</sup> (Nafion<sup>®</sup> D2020 at 80 °C), and Kreuer<sup>14</sup> (Nafion<sup>®</sup> 117 at varied temperature). Lines represent the sorption isotherms computed with equation (4) fitted to all shown experimental data.

Figure 4 shows the comparison of the back-diffusion coefficients used in membrane and CL ionomer in this work and those in the literature<sup>26–28</sup>.

## 5. Thickness and porosity of the compressed gas-diffusion layer

Since the GDL was compressed when the MEA was sandwiched between the bipolar plates, the compressed values of its thickness and porosity had to be found based on the known uncompressed values. Assuming MPL and CLs incompressible, thickness of the compressed GDL was computed as

$$L_{\text{GDL}}^{\text{comp}} = L_{\text{GDL}+\text{MPL}}^{\text{comp}} - L_{\text{MPL}},$$

where the compressed combined thickness of GDL and MPL was found as

$$L_{\text{GDL}+\text{MPL}}^{\text{comp}} = L_{\text{gasket}} - \frac{L_{\text{ACL}} + L_{\text{CCL}}}{2}.$$

Here,  $L_{\text{gasket}}$  is the thickness of a rigid gasket used in the cell assembly. The MPL thickness  $L_{\text{MPL}}$  was estimated in-house through mercury-intrusion porosimetry<sup>29</sup>. The compressed porosity of the GDL was then computed from

$$\varepsilon_{\text{V,GDL}}^{\text{comp}} = 1 - \frac{(1 - \varepsilon_{\text{V,GDL}})L_{\text{GDL}}}{L_{\text{GDL}}^{\text{comp}}}.$$

## 6. Electrical and thermal conductivity of gas-diffusion and micro-porous layers

Electrical conductivity of the MPL was estimated from the known conductivity of the separate GDL and GDL-MPL combination<sup>30</sup> (both compressed at 1 MPa) by representing the layers with a set of resistors connected either in series (for the through-plane transport) or in parallel (for the in-plane transport). Each resistance was defined as

$$R = \frac{L^*}{\sigma A},$$

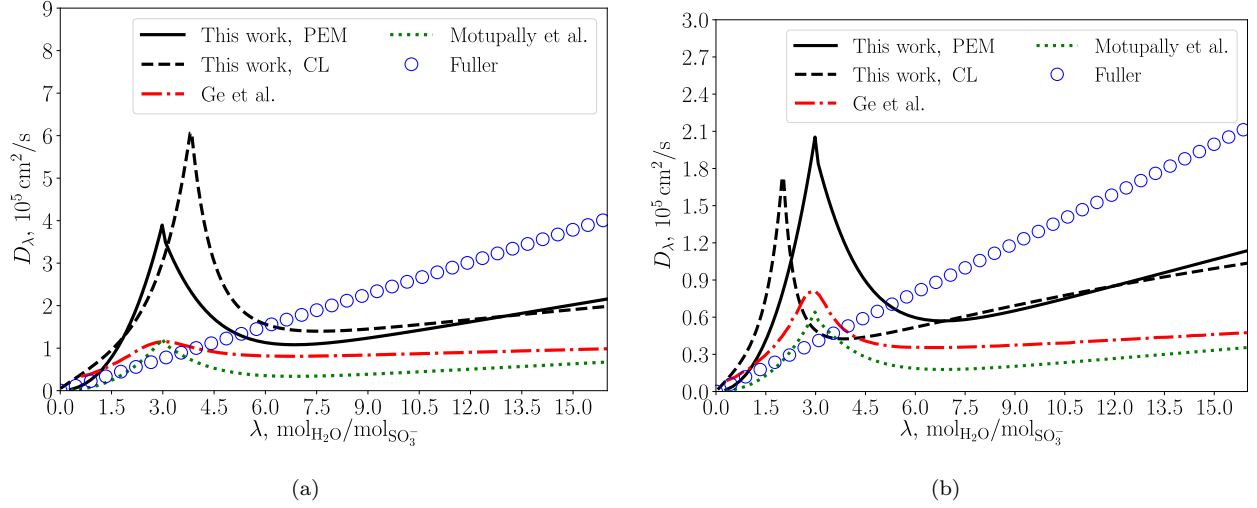


Figure 4: Comparison of the back-diffusion coefficients for water in the electrolyte used in this work to those by Ge et al.<sup>27</sup>, Motupally et al.<sup>26</sup>, and Fuller<sup>28</sup> at (a) 80 °C and (b) 50 °C. Bulk diffusivity is shown, and the effective back-diffusion coefficient was computed as  $D_{\lambda}^{\text{eff}} = \varepsilon_{\text{N}}^{1.6} D_{\lambda}$  in the catalyst layers.

where  $L^*$  is the thickness of the layer in the direction of the electron transport and  $A$  is the cross-sectional area orthogonal to that direction. The resulting equations for the through-plane and in-plane electrical conductivity of the MPL were as follows (the superscript indicating the effective transport property was omitted):

$$\sigma_{\text{s,MPL}}^{\text{TP}} = \frac{L_{\text{MPL}}}{\frac{L_{\text{GDL+MPL}}^{\text{comp}}}{\sigma_{\text{s,GDL+MPL}}^{\text{TP}}} - \frac{L_{\text{GDL}}^{\text{comp}}}{\sigma_{\text{s,GDL}}^{\text{TP}}}}, \quad (5)$$

$$\sigma_{\text{s,MPL}}^{\text{IP}} = \frac{\sigma_{\text{s,GDL+MPL}}^{\text{IP}} L_{\text{GDL+MPL}}^{\text{comp}} - \sigma_{\text{s,GDL}}^{\text{IP}} L_{\text{GDL}}^{\text{comp}}}{L_{\text{MPL}}}. \quad (6)$$

Relations (5) and (6) result in highly anisotropic conductivity of the MPL, which is believed to have an isotropic structure. However, this may be attributed to the composite sub-layer at the GDL-MPL interface<sup>31,32</sup>, the transport properties of which depend on the alignment of the GDL fibers in that region.

## 7. Input parameters

The main input parameters of the model are listed in the main text. The rest of the parameters and relations are given in Tables 1–2 and in<sup>19,33–35</sup>.

Table 1: Model parameters for the catalyst layers.

Parameter	Value/expression	Details
<b>Geometry and structure</b>		
Platinum loading on support, wt%	40	Manufacturer
Platinum loading per unit area, mg/cm <sup>2</sup>	0.1008 (anode), 0.1455 (cathode)	Controlled (inkjet printing and gravimetric measurement)
Electrolyte loading, wt%	30	Controlled (ink preparation)
Active area, cm <sup>2</sup> <sub>Pt</sub> /cm <sup>3</sup> <sub>CL</sub>	212,000	Measured (cyclic voltammetry)

Table 1: (Continued) Model parameters for the catalyst layers.

Parameter	Value/expression	Details
Support density (carbon black), g/cm <sup>3</sup>	1.69	36
Electrolyte density, g/cm <sup>3</sup>	2	33–35
Equivalent weight of the electrolyte, g/mol <sub>SO<sub>3</sub><sup>-</sup></sub>	1100	33–35
Thermal transfer		
Volumetric heat capacity of the electrolyte, kJ/(m <sup>3</sup> K)	1800 <sup>a</sup>	Refs. 17,25,37
Entropy change per mole of H <sub>2</sub> , J/(mol K)	$\Delta\bar{S}_{\text{overall}} = 4.184([8(1 + \ln(T))] - 92.84)$	35
Fraction of the overall entropy change due to ORR	$f_{\text{ORR}} = 1$	Refs. 19,35
Molar latent heat of water vaporization, J/mol	$\bar{H}_{\text{lv}} = M_{\text{H}_2\text{O}} \left( 2500.304 - 2.252T_{\text{C}} - 0.0215T_{\text{C}}^{1.5} + 3.175 \cdot 10^{-4}T_{\text{C}}^{2.5} - 2.861 \cdot 10^{-5}T_{\text{C}}^3 \right)$	Ref. 38
Molar enthalpy change due to water absorption/desorption by the electrolyte, kJ/mol	45	Refs. 19,35

<sup>a</sup> Assumed constant value withing the range used in the modeling studies<sup>17,25,37</sup>.

Table 2: Additional model parameters for the Nafion<sup>®</sup> NR-211 membrane.

Parameter	Value/expression	Details
Thickness, $\mu\text{m}$	25	Manufacturer
Density, g/cm <sup>3</sup>	2	Refs. 33–35
Equivalent weight, g/mol <sub>SO<sub>3</sub><sup>-</sup></sub>	1100	Refs. 33–35
Molar enthalpy change due to water absorption/desorption, kJ/mol	45	Refs. 19,35
Volumetric heat capacity, kJ/(m <sup>3</sup> K)	1800 <sup>a</sup>	Refs. 17,25,37

<sup>a</sup> Assumed constant value withing the range used in the modeling studies<sup>17,25,37</sup>.

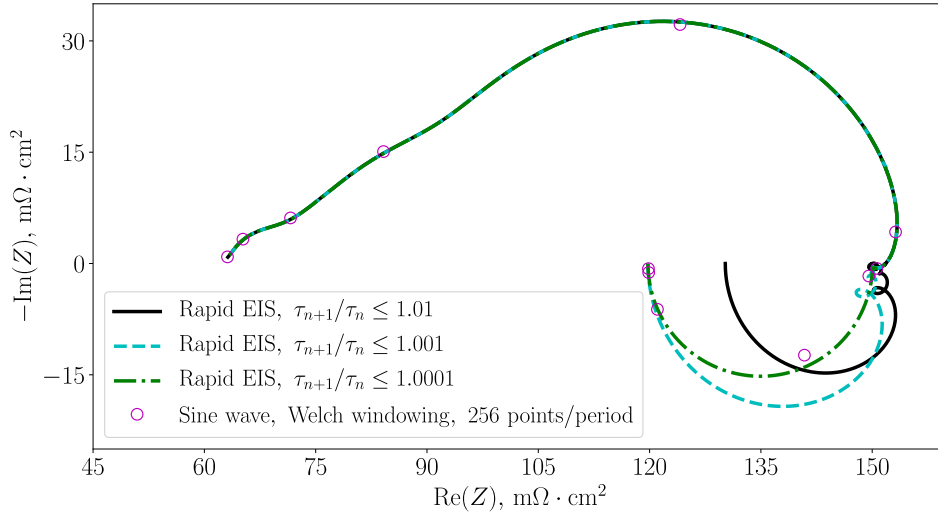
## 8. Validation of the rapid-EIS approach

The implemented rapid-EIS approach<sup>39</sup> and the non-equidistant Fourier transform<sup>40</sup> were validated by comparing the resulting impedance spectra to those found with the conventional sine-wave approach. Figure 5(c) shows a comparison between the two approaches. Three different time-scale resolutions were considered in the rapid-EIS simulations by limiting the maximum ratio of the current to the previous time-step size  $\tau_{n+1}/\tau_n$  to 1.01, 1.001, and 1.0001 (1, 0.1, and 0.01% increase between the time layers, respectively). All spectra exhibited excellent agreement in the capacitive domain, but deviated from each other in the low-frequency inductive loop.

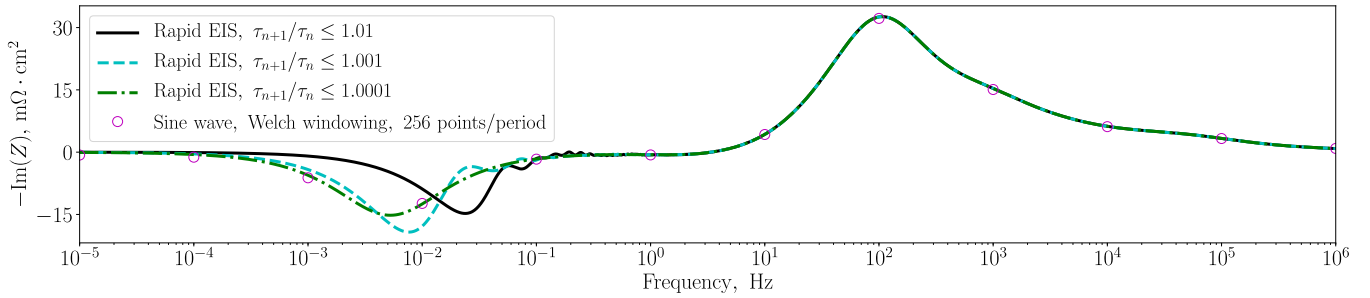
The rapid-EIS spectrum with the highest time-scale resolution was the most accurate; however, it required about 27 days of computation. The significant computational time may be a shortcoming of the first-order-accurate implicit Euler method used in this work and the Richardson extrapolation algorithm that increases the temporal accuracy at the cost of solving the problem thrice to compute each time layer. The lowest-resolution case required 7 hours of computation, but had the highest uncertainty in approximating the characteristic frequency and the size of the inductive loop. Since the primary interest of this work is in the effect of the different physical phenomena on the relative change in the inductive loop rather than on accurately predicting its size, the case with the medium time-scale resolution ( $\tau_{n+1}/\tau_n \leq 1.001$ ), which took about 65 hours of the computational time, was considered optimal and was used in all EIS studies shown in this work. The frequency range of the main inductive behavior, 0.1–200 mHz, was resolved correctly in this case, as seen in Figure 5(c). The minor inductive loop at 0.2–5 Hz was time-step-size-independent among the considered cases, and thus was computed accurately.

The local impedance oscillations at 0.02–1 Hz observed in the two coarser time-discretization cases in Figure 5 are not present in the finer case, which indicates that they are a numerical artifact.

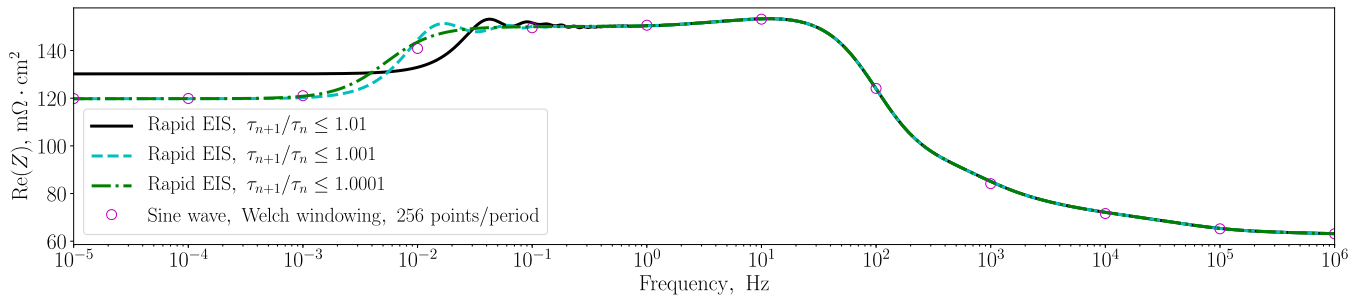
Sine-wave simulations were performed by generating 13 periods of a sinusoidal wave in voltage at the given single frequency. A Welch window<sup>41</sup> was applied to the current-density signal, which was then processed with the Fast Fourier Transform (FFT) algorithm from SciPy<sup>10</sup>. Since the input voltage signal was known and had a single frequency component, no FFT processing was performed on it. Convergence studies were performed on the resulting phase angle and frequency of the current-density signal, and the imaginary and real parts of the impedance. It was found that using 256 equidistant nodal points per period of the wave was optimal in terms of the achieved accuracy of the results and the computational time. Since each sine-wave simulation took between 1.5 and 2.5 hours per frequency, the overall computational time may reach and exceed that for the rapid-EIS approach depending on the desired frequency resolution of the spectrum. This is because the frequencies are analyzed after a rapid-EIS simulation is complete, and thus any number of frequencies can be extracted from a single simulation (to a certain extent where aliasing may start to occur).



(a)



(b)



(c)

Figure 5: Comparison of the impedance spectra obtained with the rapid-EIS approach using three different time-scale resolutions to the spectrum computed using the sine-wave approach: (a) Nyquist plot; (b) Bode plot of the negative imaginary part; (c) Bode plot of the real part.

## References

- [1] A. Kusoglu, A. Kwong, K. T. Clark, H. P. Gunterman, A. Z. Weber, Water uptake of fuel-cell catalyst layers, *Journal of The Electrochemical Society* 159 (9) (2012) F530–F535 (2012).
- [2] C.-Y. Jung, S.-C. Yi, Influence of the water uptake in the catalyst layer for the proton exchange membrane fuel cells, *Electrochemistry Communications* 35 (2013) 34–37 (2013).
- [3] H. Iden, K. Sato, A. Ohma, K. Shinohara, Relationship among microstructure, ionomer property and proton transport in pseudo catalyst layers, *Journal of The Electrochemical Society* 158 (8) (2011) B987–B994 (2011).
- [4] G. C. Abuin, M. C. Fuertes, H. R. Corti, Substrate effect on the swelling and water sorption of Nafion nanomembranes, *Journal of membrane science* 428 (2013) 507–515 (2013).
- [5] A. Kusoglu, D. Kushner, D. K. Paul, K. Karan, M. A. Hickner, A. Z. Weber, Impact of substrate and processing on confinement of Nafion thin films, *Advanced Functional Materials* 24 (30) (2014) 4763–4774 (2014).
- [6] H. K. Shim, D. K. Paul, K. Karan, Resolving the contradiction between anomalously high water uptake and low conductivity of nanothin Nafion films on SiO<sub>2</sub> substrate, *Macromolecules* 48 (22) (2015) 8394–8397 (2015).
- [7] H. K. Shim, Water sorption properties of sub-micron thin ionomer films, Master’s thesis, Queen’s University (2016).
- [8] U. N. Shrivastava, H. Fritzsche, K. Karan, Interfacial and bulk water in ultrathin films of Nafion, 3M PFSA, and 3M PFIA ionomers on a polycrystalline platinum surface, *Macromolecules* 51 (23) (2018) 9839–9849 (2018).
- [9] A. Kongkanand, Interfacial water transport measurements in Nafion thin films using a quartz-crystal microbalance, *The Journal of Physical Chemistry C* 115 (22) (2011) 11318–11325 (2011).
- [10] SciPy Reference Guide, <https://docs.scipy.org/doc/scipy/reference/>. Accessed December 19, 2019. (2019).
- [11] T. A. Zawodzinski Jr, M. Neeman, L. O. Sillerud, S. Gottesfeld, Determination of water diffusion coefficients in perfluorosulfonate ionomeric membranes, *The Journal of Physical Chemistry* 95 (15) (1991) 6040–6044 (1991).
- [12] C. K. Mittelsteadt, H. Liu, Conductivity, permeability, and ohmic shorting of ionomeric membranes, in: W. Vielstich, H. A. Gasteiger, H. Yokokawa (Eds.), *Handbook of fuel cells: Fundamentals technology and applications: Advances in electrocatalysis, materials, diagnostics and durability*, Springer New York, John Wiley & Sons, 2009, pp. 345–358 (2009).
- [13] J. T. Hinatsu, M. Mizuhata, H. Takenaka, Water uptake of perfluorosulfonic acid membranes from liquid water and water vapor, *Journal of the Electrochemical Society* 141 (6) (1994) 1493–1498 (1994).
- [14] K.-D. Kreuer, The role of internal pressure for the hydration and transport properties of ionomers and polyelectrolytes, *Solid State Ionics* 252 (2013) 93–101 (2013).

- [15] A. Kusoglu, A. Z. Weber, New insights into perfluorinated sulfonic-acid ionomers, *Chemical reviews* 117 (3) (2017) 987–1104 (2017).
- [16] T. Springer, T. Zawodzinski, S. Gottesfeld, Polymer electrolyte fuel cell model, *Journal of the Electrochemical Society* 138 (8) (1991) 2334–2342 (1991).
- [17] A. Shah, G.-S. Kim, P. Sui, D. Harvey, Transient non-isothermal model of a polymer electrolyte fuel cell, *Journal of Power Sources* 163 (2) (2007) 793–806 (2007). doi:10.1016/j.jpowsour.2006.09.022.
- [18] A. Vorobev, O. Zikanov, T. Shamim, A computational model of a PEM fuel cell with finite vapor absorption rate, *Journal of Power Sources* 166 (1) (2007) 92–103 (2007).
- [19] M. Bhaiya, A. Putz, M. Secanell, Analysis of non-isothermal effects on polymer electrolyte fuel cell electrode assemblies, *Electrochimica Acta* 147 (2014) 294–309 (2014).
- [20] G. Zhang, L. Fan, J. Sun, K. Jiao, A 3D model of PEMFC considering detailed multiphase flow and anisotropic transport properties, *International Journal of Heat and Mass Transfer* 115 (2017) 714–724 (2017).
- [21] J. Zhou, A. Putz, M. Secanell, A mixed wettability pore size distribution based mathematical model for analyzing two-phase flow in porous electrodes I. Mathematical model, *Journal of The Electrochemical Society* 164 (6) (2017) F530–F539 (2017).
- [22] Z. Zhan, H. Zhao, P. C. Sui, P. Jiang, M. Pan, N. Djilali, Numerical analysis of ice-induced stresses in the membrane electrode assembly of a PEM fuel cell under sub-freezing operating conditions, *International Journal of Hydrogen Energy* 43 (9) (2018) 4563–4582 (2018).
- [23] J. Zhou, S. Shukla, A. Putz, M. Secanell, Analysis of the role of the microporous layer in improving polymer electrolyte fuel cell performance, *Electrochimica Acta* 268 (2018) 366–382 (2018).
- [24] S. Li, J. Yuan, G. Xie, B. Sundén, Effects of agglomerate model parameters on transport characterization and performance of PEM fuel cells, *International Journal of Hydrogen Energy* 43 (17) (2018) 8451–8463 (2018).
- [25] A. Goshtasbi, P. García-Salaberri, J. Chen, K. Talukdar, D. G. Sanchez, T. Ersal, Through-the-membrane transient phenomena in PEM fuel cells: A modeling study, *Journal of The Electrochemical Society* 166 (7) (2019) F3154–F3179 (2019).
- [26] S. Motupally, A. J. Becker, J. W. Weidner, Diffusion of water in Nafion 115 membranes, *Journal of The Electrochemical Society* 147 (9) (2000) 3171–3177 (2000).
- [27] S. Ge, X. Li, B. Yi, I.-M. Hsing, Absorption, desorption, and transport of water in polymer electrolyte membranes for fuel cells, *Journal of the Electrochemical Society* 152 (6) (2005) A1149–A1157 (2005).
- [28] T. F. Fuller, Solid-polymer-electrolyte fuel cells, Ph.D. thesis, University of California, Berkeley (1992).
- [29] S. Shukla, F. Wei, M. Mandal, J. Zhou, M. Saha, J. Stumper, M. Secanell, Determination of PEFC gas diffusion layer and catalyst layer porosity utilizing Archimedes principle, *Journal of The Electrochemical Society* (2019).

- [30] R. Schweiss, C. Meiser, T. Damjanovic, I. Galbiati, N. Haak, SIGRACET gas diffusion layers for PEM fuel cells, electrolyzers and batteries, White paper SGL Group (2016).
- [31] O. S. Burheim, G. A. Crymble, R. Bock, N. Hussain, S. Pasupathi, A. du Plessis, S. le Roux, F. Seland, H. Su, B. G. Pollet, Thermal conductivity in the three layered regions of micro porous layer coated porous transport layers for the pem fuel cell, *international journal of hydrogen energy* 40 (46) (2015) 16775–16785 (2015).
- [32] R. Bock, A. Shum, T. Khoza, F. Seland, N. Hussain, I. V. Zenyuk, O. S. Burheim, Experimental study of thermal conductivity and compression measurements of the gdl-ipl interfacial composite region, *ECS Transactions* 75 (14) (2016) 189–199 (2016).
- [33] M. Secanell, Computational modeling and optimization of proton exchange membrane fuel cells, Ph.D. thesis, University of Victoria (2007).
- [34] M. Secanell, R. Songprakorp, A. Suleman, N. Djilali, Multi-objective optimization of a polymer electrolyte fuel cell membrane electrode assembly, *Energy & Environmental Science* 1 (3) (2008) 378–388 (2008).
- [35] M. Bhaiya, An open-source two-phase non-isothermal mathematical model of a polymer electrolyte membrane fuel cell, Master’s thesis, University of Alberta (2014).
- [36] S. Shukla, D. Stanier, M. Saha, J. Stumper, M. Secanell, Analysis of inkjet printed PEFC electrodes with varying platinum loading, *Journal of The Electrochemical Society* 163 (7) (2016) F677–F687 (2016).
- [37] J. Ko, H. Ju, Comparison of numerical simulation results and experimental data during cold-start of polymer electrolyte fuel cells, *Applied energy* 94 (2012) 364–374 (2012).
- [38] C. Popiel, J. Wojtkowiak, Simple formulas for thermophysical properties of liquid water for heat transfer calculations (from 0 c to 150 c), *Heat transfer engineering* 19 (3) (1998) 87–101 (1998).
- [39] W. G. Bessler, Rapid impedance modeling via potential step and current relaxation simulations, *Journal of The Electrochemical Society* 154 (11) (2007) B1186–B1191 (2007).
- [40] H. Wiese, K. G. Weil, An efficient fourier transform algorithm for frequency domains of several decades using logarithmically spaced time samples, *IEEE Transactions on Acoustics, Speech, and Signal Processing* 36 (7) (1988) 1096–1099 (1988).
- [41] W. H. Press, S. A. Teukolsky, W. T. Vetterling, B. P. Flannery, *Numerical recipes: The art of scientific computing*, 3rd Edition, Cambridge University Press, 2007 (2007).